Dynamic Structures of Phosphodiesterase-5 Active Site by Combined Molecular Dynamics Simulations and Hybrid Quantum Mechanical/Molecular Mechanical Calculations

YING XIONG,[1,2] HAI-TING LU,[1,2] CHANG-GUO ZHAN[2]

[1]*Key Laboratory of Pesticide and Chemical Biology of Ministry of Education, College of Chemistry, Central China Normal University, Wuhan 430079, People's Republic of China*

[2]*Department of Pharmaceutical Sciences, College of Pharmacy, University of Kentucky, Lexington, Kentucky 40536*

Received 21 May 2007; Revised 30 October 2007; Accepted 1 November 2007

DOI 10.1002/jcc.20888

Published online 27 December 2007 in Wiley InterScience (www.interscience.wiley.com).

Abstract: Various quantum mechanical/molecular mechanical (QM/MM) geometry optimizations starting from an x-ray crystal structure and from the snapshot structures of constrained molecular dynamics (MD) simulations have been performed to characterize two dynamically stable active site structures of phosphodiesterase-5 (PDE5) in solution. The only difference between the two PDE5 structures exists in the catalytic, second bridging ligand (BL2) which is HO^- or H_2O. It has been shown that, whereas BL2 (i.e. HO^-) in the PDE5(BL2 = HO^-) structure can really bridge the two positively charged metal ions (Zn^{2+} and Mg^{2+}), BL2 (i.e. H_2O) in the PDE5(BL2 = H_2O) structure can only coordinate Mg^{2+}. It has been demonstrated that the results of the QM/MM geometry optimizations are remarkably affected by the solvent water molecules, the dynamics of the protein environment, and the electronic embedding charges of the MM region in the QM part of the QMM/MM calculation. The PDE5(BL2 = H_2O) geometries optimized by using the QM/MM method in different ways show strong couplings between these important factors. It is interesting to note that the PDE5(BL2 = HO^-) and PDE5(BL2 = H_2O) geometries determined by the QM/MM calculations neglecting these three factors are all consistent with the corresponding geometries determined by the QM/MM calculations that account for all of these three factors. These results suggest the overall effects of these three important factors on the optimized geometries can roughly cancel out. However, the QM/MM calculations that only account for some of these factors could lead to considerably different geometries. These results might be useful also in guiding future QM/MM geometry optimizations on other enzymes.

 J Comput Chem 29: 1259–1267, 2008

Key words: enzyme; active site structure; molecular dynamics; QM/MM; protein dynamics; metalloenzyme

Introduction

Cyclic nucleotide phosphodiesterases (PDEs) are a superfamily of enzymes responsible for the hydrolysis of cyclic adenosine 3′,5′-monophosphate (cAMP) and cyclic guanosine 3′,5′-monophosphate (cGMP) that are important intracellular second messengers playing a central role in regulating many relevant cell functions.[1–5] The human genome encodes 21 PDE genes and over 60 PDE isoforms categorized into 11 families (PDE1 to PDE11).[1,6] PDE4, PDE7, and PDE8 are highly specific for cAMP, whereas PDE5, PDE6, and PDE9 are highly specific for cGMP. PDE1, PDE2, PDE3, PDE10, and PDE11 exhibit dual specificity with greater or lesser preference for cAMP or cGMP.[7] Thus, PDEs are clinical targets for such biological disorders as retinal degeneration, congestive heart failure, depression, asthma, erectile dysfunction, and inflammation.[8–14] Among the 11 different PDE families, PDE5 is the primary target for the development of small molecules, such as the well-known sildenafil (Viagra), vardenafil (Levitra), and tadalafil (Cialis), to treat male erectile dysfunction (ED).[15–18] Understanding the protein structures of PDE5, particularly the active site structures, and catalytic mechanism will provide a solid basis for rational design of novel, more potent inhibitors of PDE5.

Correspondence to: C.-G. Zhan; e-mail: zhan@uky.edu

Contract/grant sponsor: National Natural Science Foundation of China; contract/grant numbers: 20602014, 20503008, 20528201

Contract/grant sponsor: NIH; contract/grant number: R01DA013930

Contract/grant sponsor: Center for Computational Sciences, University of Kentucky

PDE5A is the only subtype of PDE5 reported, and there are four isoforms (PDE5A1-4).[19] The catalytic domains of these splicing variants are exactly the same. Sung et al.[19] first reported 3D X-ray crystal structures of the catalytic domain (residues 537 to 860) of a cGMP-specific human PDE5 complexed with three drug molecules, i.e. sildenafil (Viagra), tadalafil (Cialis), and vardenafil (Levitra). These PDE5 crystal structures consistently demonstrate that the active site of PDE5 is located at the center of the C-terminal helical bundle domain.[19,20–22] The substrate pocket is ~10 Å deep, with a narrow opening and a wide inner space, giving a total volume of ~330 Å^3. It is composed of four subsites (shown in Chart 1): a metal-binding site (M site), core pocket (Q pocket), hydrophobic pocket (H pocket), and lid region (L region). The M site contains both a zinc ion (Zn^{2+}) and a second metal ion (Mg^{2+}) and is surrounded by helices a6, a8, a9, a10, and a12.[7] The first bridging ligand was clearly Asp654. However, the second bridging ligand (BL2) was described as a water molecule in all of these PDE5 crystal structures. In fact, it was uncertain whether BL2 is a water molecule or a hydroxide ion because hydrogen atoms cannot be determined by an X-ray diffraction technique regardless of the resolution of the X-ray crystal structure. Such a structural problem is also difficult to solve by using other existing experimental approaches. For example, biochemical experiments would not be able to directly determine whether BL2 should be a water molecule or a hydroxide ion without using any hypothesis. Nuclear magnetic resonance (NMR), in principle, might be a potentially useful approach to solve such a structural problem, but no NMR study on such a bridging ligand (water molecule versus hydroxide ion) has ever been reported as far as we know.

The determination of the structural identity of BL2 is crucial for understanding the catalytic mechanisms of PDE5, for studying enzyme–ligand (substrate or inhibitor) binding, and for future rational design of novel drugs targeting PDE5. For example, different answers to this question may point to different possible nucleophiles attacking the phosphorus center of the substrate (cGMP) to initialize the catalytic reaction. In addition, the structural identity of BL2 should also affect the PDE5 binding with substrates and inhibitors, as different structural forms (neutral H_2O or negatively charged HO^-) of BL2 would provide different electrostatic potentials affecting PDE5 binding with a substrate or inhibitor. Thus, a drug design and discovery effort based on an incorrect structural identity of BL2 could only lead to meaningless predictions.

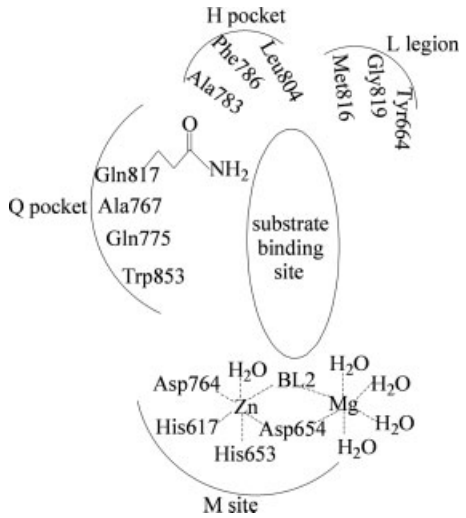

Chart 1. A schematic representation of the PDE5 active site.

Recently, the combined quantum mechanical/molecular mechanical (QM/MM) approach has become the popular method of choice for modeling biomacromolecular systems.[23] QM/MM energy expression contains subtractive and additive schemes. IMOMM method by Maseras and Morokuma[24] is an example for substractive QM/MM scheme. Its main advantage is simplicity and its disadvantage is requirement of a complete set of MM parameters for the atoms in the QM region. On the contrary, MM parameters for the atoms in the QM region are not needed for the additive schemes, but it is challenging for these additive schemes to deal with interaction energy between the QM region and MM region. QM/MM approach has been proved to be a good method in determining ligand identities in the active-sites.[25,26] In these two interesting studies, by using the combined QM/MM method and X-ray diffraction data, a QM/MM/X-ray refinement was performed to get reliable structural information which is difficult to be solved only with experimental approaches.

To determine the structural identity of BL2 in the PDE5 active site, we previously carried out two sets of molecular dynamics (MD) simulations and hybrid QM/MM calculations[27] on the PDE5 structure resolved by the X-ray diffraction. The MD simulations were performed in a water bath, whereas the QM/MM geometry optimizations were carried out in the gas phase by using the default ONIOM approach implemented in the Gaussian03 program.[28] The two sets of MD simulations and QM/MM calculations started from the same X-ray crystal structure, but BL2 was considered to be HO^- in one set of simulations/calculations and H_2O in the other set of simulations/calculations. Both the MD simulations and QM/MM calculations revealed that only HO^- (as BL2) can bridge the two positively charged metal ions, whereas H_2O only coordinated one metal ion and left the other metal ion during the MD simulation and QM/MM geometry optimization processes. So, only when BL2 = HO^-, the simulated and optimized PDE5 structures were consistent with the X-ray crystal structure, suggesting that BL2 in the PDE5 active site in the X-ray crystal structure should be HO^- rather than H_2O. In solution, both the PDE5(BL2 = HO^-) and PDE5(BL2 = H_2O) structures could coexist, with a higher concentration of PDE5(BL2 = HO^-) in a high-pH solution or with a higher concentration of PDE5(BL2 = H_2O) in a low-pH solution.

There were some possible questions concerning the previous QM/MM geometry optimizations used to determine the structural identify of BL2 in the PDE5 active site. First of all, the previous QM/MM geometry optimizations were performed in the gas phase, without accounting for the effects of solvent water molecules that do not directly coordinate the metal ions. The question is whether the neglected solvent water can dramatically change the coordination of BL2 or not. Further, the default ONIOM approach implemented in the Gaussian03 program does

not include the electronic embedding charges of the MM region in the QM part of QM/MM calculation. The question is whether the partial atomic charges of the MM atoms can significantly affect the geometries determined by the QM/MM calculations. In addition, the previous QM/MM geometry optimization starting from the X-ray crystal structure for a given identity of BL2 could only provide a local-minimum structure of the protein. Does the optimized local-minimum structure reasonably reflect the true, dynamically stable protein structure in solution?

To answer these critical questions, we have carried out more extensive and contrastive QM/MM calculations using various options, including the QM/MM geometry optimizations starting from different snapshots of MD-simulated structures. The combined MD simulations and QM/MM calculations enable us to appropriately account for the protein dynamics in the QM/MM geometry optimizations on the PDE5 structures. The results obtained from these MD simulations and QM/MM calculations have led to reliable new insights into the PDE5 active site structures both in the crystal structure and in solution.

Computational Methods

Molecular Dynamics Simulation

The initial PDE5 structures used in our MD simulations were built from the corresponding X-ray crystal structure deposited in the Protein Data Bank[29] (pdb code: 1RKP) which was also used as the initial structure for all of the calculations on PDE5 in our previous study.[27] The standard protonation states at physiological condition (pH ~7.4) were set to all ionizable residues, and the proton was set on the N_ε atom for all His residues as His617 and His653 side chains of PDE5 all coordinate the Zn^{2+} ion through the other nitrogen atom (denoted by N_η). Amber7 program suite[30] was used to perform the MD simulations in this study. The partial atomic charges for the non-residue atoms of hydroxide ion were calculated by using the restricted electrostatic-potential (RESP) fitting protocol implemented in the Antechamber module of the Amber7 program following electrostatic potential (ESP) calculations at *ab initio* HF/6-31G* level. For example, the RESP charges used for HO^- were calculated at the HF/6-31G* level to be −1.206 and 0.206 for the O and H atoms, respectively. The initial structure was neutralized by adding counterions and was solvated in a rectangular box of TIP3P water molecules with a minimum solute-wall distance of 10 Å. Specifically, the net charge is 0 for the PDE5 structure when BL2 = HO^- and +1 for the PDE5 structure when BL2 = H_2O. Hence, one Cl^- was added to neutralize the solvated PDE5(BL2 = H_2O) system. The total number of atoms in each solvated protein structure for the MD simulations was more than 40,000, although the total number of atoms of each PDE5 structure was only about 5000. The MD simulations performed in the present MD simulations were somewhat different from our previous MD simulations[27] on the PDE5 structures in terms of the initial positions of the solvent water molecules that do not directly coordinate the metal ions. In the previous MD simulations, the X-ray crystal structure was only used to obtain the initial atomic coordinates of the amino acid residues, metal ions, and the nonstandard residues (H_2O and HO^-) that directly coordinate the metal ions. All of the solvent water molecules that do not directly coordinate the metal ions were added automatically by using the Amber7 program. In the present MD simulations, the coordinates of all atoms in the X-ray crystal structure were kept and we only needed to add the additional solvent water molecules to the used rectangular box.

The general procedure for carrying out the MD simulations in water was essentially the same as that used in our previous MD simulations on PDE5 and other similar protein systems containing a bimetallic active site[27,31] with one exception that the internuclear distances between the oxygen atom of BL2, denoted by O(BL2), and the two metal ions were constrained during the MD simulations in the present study. The nonbonded models were used for the metal ions. The MD simulations in this study were performed by using the Sander module of the Amber7 program. The protein-solvent system was optimized prior to the simulation as follows. First, the protein was frozen and the solvent molecules with counterions were allowed to move during a 3000-step minimization. Second, all the atoms were allowed to relax by a 3000-step full minimization. After full relaxation, the protein was frozen and the solvent molecules with the counterions were allowed to move during a 2500-step MD simulation. Then, relaxing all the atoms, the system was slowly heated to 250 K in 20 ps and then to 298.15 K in 80 ps. The production MD simulation at T = 298.15 K was kept running until we believed that a stable MD trajectory had been obtained for each of the simulated structures. The time step used for the MD simulations was 2 fs. Periodic boundary conditions in the constant pressure and temperature (NPT) ensemble (i.e. isothermal-isobaric ensemble) at T = 298.15 K with Berendsen temperature coupling[32] and P = 1 atm with isotropic molecule-based scaling[32] were applied. The SHAKE algorithm[33] was used to fix all covalent bonds containing a hydrogen atom. The nonbonded pair list was updated every 10 steps. The particle mesh Ewald (PME) method[34] was used to treat long-range electrostatic interactions. A residue-based cutoff of 10 Å was utilized to the non-covalent interactions. The coordinates of the simulated systems were collected every 1 ps during the production MD stages.

QM/MM Calculation

The ONIOM-based QM/MM approach[35] implemented in the Gaussian03 program[28] was used to fully optimize geometries of the PDE5 structures. Two layers were defined in each of our ONIOM-based QM/MM calculations: the high layer (including the metal ions and atoms from all ligands coordinating the metal ions; see later for the specific high-layer atoms depicted as the balls in the Figures) was treated quantum mechanically at the B3LYP/6-31G* level and the low layer (for the remaining part of the solvated protein system) was treated molecular mechanically by using the Amber force field as used in our MD simulations with the Amber7 program. Some missing force field parameters (including the RESP charges for HO^- and van der Waals parameters for Zn^{2+} and Mg^{2+}) were added before running the QM/MM calculations with ONIOM approach. The van der Waals parameters for Zn^{2+} and Mg^{2+} came from the "parm99.dat" data file of the Amber force field[30]; these

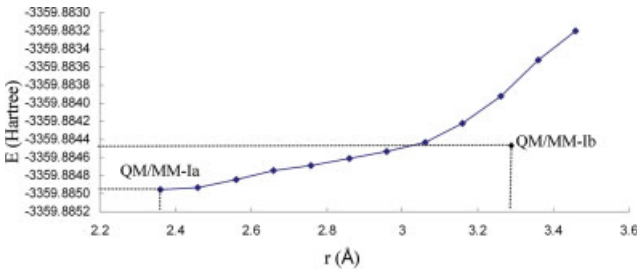

Figure 1. Plot of the total energy (in Hartree) of PDE5(BL2 = H_2O) calculated at the B3LYP/6-31G* level for a partially optimized geometry (with the QM/MM-Ib geometry optimization starting from the QM/MM-Ia structure) versus the Zn^{2+}-O(H_2O) distance frozen. Marked in the figure are the energies and Zn^{2+}-O(H_2O) distances in the two fully-optimized geometries corresponding to QM/MM-Ia and QM/MM-Ib (all with electronic embedding). [Color figure can be viewed in the online issue, which is available at www.interscience.wiley.com.]

parameters were missing in the "parm96.dat" data file adopted by the Gaussian03.[28] The QM/MM calculations were performed (using either the X-ray crystal structure or a snapshot of the MD-simulated structure) in two different ways: the QM part of the QM/MM calculation was carried out with and without the electronic embedding charges, i.e. the partial atomic charges of the MM atoms that have no bonded interactions with the QM atoms. During ONIOM calculation, all atoms in the standard residues kept their atomic charges from the used Amber force field whereas the charges of the metal atoms were all +2 and our calculated RESP charges were used for HO^- (i.e. −1.206 and 0.206 for the O and H atoms, respectively).

All the MD simulations and QM/MM calculations were performed on an HP's Superdome supercomputer (a shared-memory system with a total of 256 processors and parallel computing) at University of Kentucky Center for Computational Sciences and on a 34-processors IBM x335 Linux cluster (with parallel computing) in our own lab.

Results and Discussion

The Structure of PDE5(BL2 = H_2O)

The question to be addressed here is whether a water molecule BL2 (i.e. when BL2 = H_2O) can bridge the two positively charged metal ions or not in the PDE5 active site. To examine this structural problem, three contrastive sets of QM/MM calculations were performed on PDE5(BL2 = H_2O) in the present study.

As mentioned above, our previous QM/MM geometry optimization[27] starting from the X-ray crystal structure was performed in the gas phase (i.e. without keeping the solvent water molecules that do not directly coordinate the metal ions) by using the default ONIOM approach (without including the electronic embedding charges of the MM region in the QM part of the QM/MM calculation). Such type of QM/MM geometry optimization led to a PDE5(BL2 = H_2O) structure in which the optimized Mg^{2+}-O(BL2) distance is 2.00 Å and the optimized Zn^{2+}-O(BL2) distance is 3.58 Å.[27] The optimized PDE5(BL2 = H_2O) structure meant that BL2 only coordinated Mg^{2+}. In the present study, we first added the electronic embedding charges of the MM region to the QM part of the QM/MM calculation in order to examine the effects of the electronic embedding charges on the coordination of BL2. It turned out that the geometry optimization including the electronic embedding charges in the QM part of the QM/MM calculation, denoted by QM/MM-Ia (electronic embedding), led to a remarkably different PDE5(BL2 = H_2O) active site structure in which the optimized Mg^{2+}-O(BL2) distance is 2.15 Å and the optimized Zn^{2+}-O(BL2) distance is 2.36 Å. According to this new geometry obtained, when BL2 = H_2O, BL2 can also bridge the two metal ions, which seems to suggest that the previous conclusion about the PDE5(BL2 = H_2O) structure[27] was wrong. However, geometry optimizations for a large system often lead to different local minima, even with some relatively small changes in the starting geometry or optimization procedure. To test the stability of the PDE5(BL2 = H_2O) structure, we carried out a series of partial geometry optimizations starting from the PDE5(BL2 = H_2O) geometry determined by the QM/MM-Ia (electronic embedding) calculation. For each partial geometry optimization, the Zn-O(BL2) distance was elongated a little bit and frozen while all of the other geometric parameters were optimized. Depicted in Figure 1 is a plot of the total QM/MM energy (in Hartree) calculated at the B3LYP/6-31G* level for the partially optimized PDE5(BL2 = H_2O) geometry versus the Zn-O(BL2) distance. As seen in Figure 1, the total energy of PDE5(BL2 = H_2O) gradually increases while the Zn-O(BL2) distance increases. A full geometry optimization, denoted by QM/MM-Ib (electronic embedding), starting from the final partially optimized PDE5(BL2 = H_2O) geometry (at the last point depicted in Fig. 1) led to a different local-minimum geometry of (Fig. 2) PDE5(BL2 = H_2O), with an optimized Mg^{2+}-O(BL2) distance of 2.07 Å and an optimized Zn-O(BL2) distance of 3.28 Å. The total energy of the PDE5(BL2 = H_2O) geometry determined by the QM/MM-Ia (electronic embedding) is −3359.88495 Hartree, which is slightly lower than that (3359.88451 Hartree) of the PDE5(BL2 = H_2O) geometry determined by the QM/MM-Ib (electronic embedding). The energy difference is <0.3 kcal/mol. These data demonstrate that one could get different local minima starting from different initial structures and, therefore, the initial protein arrangement is important for the QM/MM geometry optimization. In addition, some other important factors, including the neglected solvent water molecules, affecting the coordination of BL2 still have not been accounted for in the QM/MM calculations.

To account for the effects of the solvent water molecules neglected in the above QM/MM calculations, we carried out other two types of geometry optimizations (with and without the electronic embedding charges) on PDE5(BL2 = H_2O) that also contains all of the nonstandard residues (including all of the water molecules) in the X-ray crystal structure. These two types of QM/MM geometry optimizations produced considerably different structures of the PDE5(BL2 = H_2O) active site. For the QM/MM calculation without the electronic embedding charges,

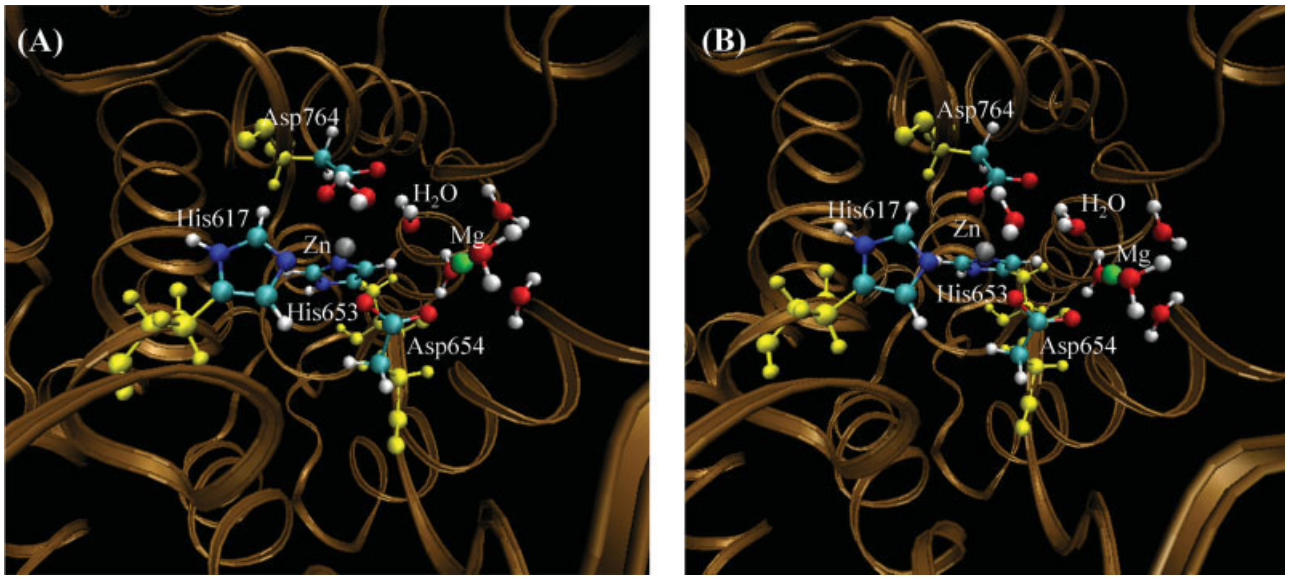

Figure 2. Geometries of PDE5(BL2 = H_2O) optimized by performing the QM/MM (electronic embedding) calculations at the B3LYP/6-31G*:Amber level. The high-layer atoms are represented by the balls in colors other than yellow. The yellow balls represent the low-layer atoms of the residues coordinating the metal ions. The sticks refer to the solvent water molecules in the active site. (A) QM/MM-Ia, i.e. the QM/MM (electronic embedding) geometry optimization in the gas phase starting from the X-ray crystal structure and neglecting solvent water molecules that do not directly coordinate the metal ions. (B) QM/MM-Ib, i.e. the QM/MM (electronic embedding) geometry optimization starting from the final partially optimized geometry (the final point in Fig. 1).

the optimized Mg^{2+}-O(BL2) distance is 2.00 Å and the optimized Zn^{2+}-O(BL2) distance is 4.05 Å. For the QM/MM calculation with the electronic embedding charges, the optimized Mg^{2+}-O(BL2) distance is 2.13 Å and the optimized Zn^{2+}-O(BL2) distance is 2.82 Å. These results clearly show that both the solvent water molecules and the electronic embedding charges are very important for determining the coordination of BL2. The Zn^{2+}-O(BL2) distance of 4.05 Å optimized without the electronic embedding charges clearly suggests that BL2 did not coordinate Zn^{2+} in the optimized PDE5(BL2 = H_2O) geom-

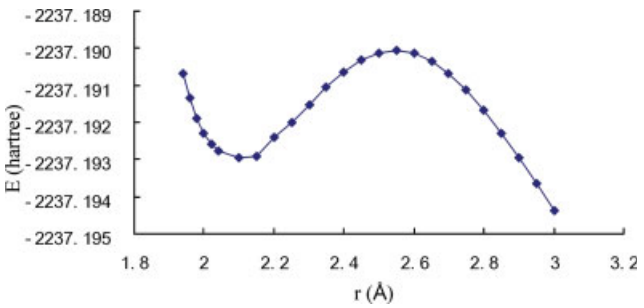

Figure 3. Plot of the total energy (in Hartree) calculated at the B3LYP/6-31G* level for a partially optimized $Zn^{2+}(H_2O)_6$ complex structure versus the Zn^{2+}-O(H_2O) distance between the subsystem $Zn^{2+}(H_2O)_5$ and the sixth water molecule. [Color figure can be viewed in the online issue, which is available at www.interscience.wiley.com.]

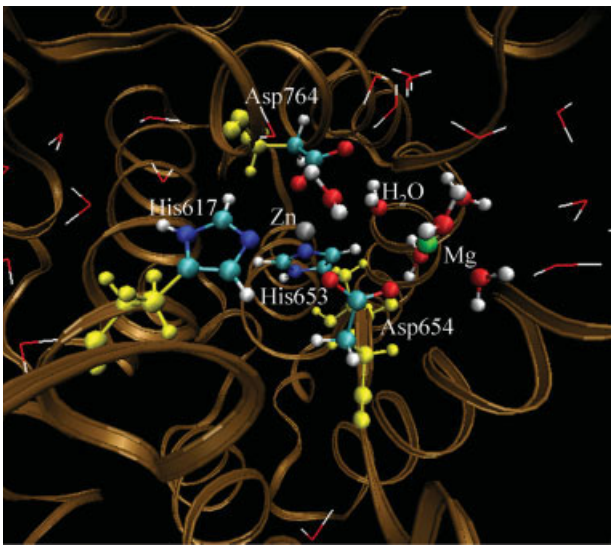

Figure 4. Geometry of the PDE5(BL2 = H_2O) optimized by performing the QM/MM (electronic embedding) calculations at the B3LYP/6-31G*:Amber level. The geometry optimization started from the X-ray crystal structure and included all of the resolved solvent water molecules in the QM/MM calculation. The high-layer atoms are represented by the balls in colors other than yellow. The yellow balls represent the low-layer atoms of the residues coordinating the metal ions. The sticks refer to the solvent water molecules in the active site.

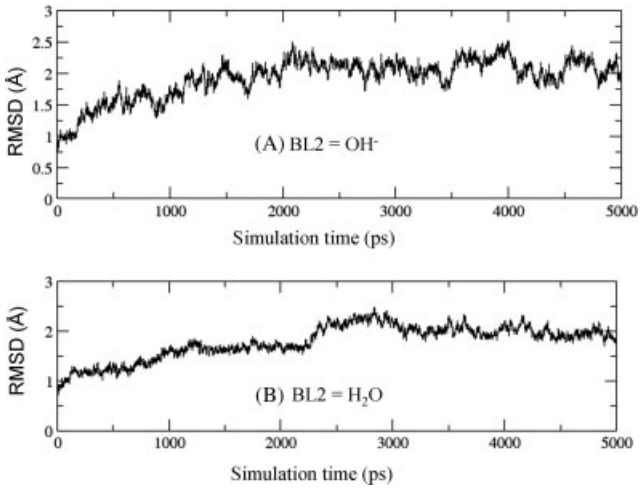

Figure 5. Plots of RMSD (in Å) versus the simulation time in the MD-simulated PDE5 structures. RMSD represents the root-mean-square deviation (in Å) of the simulated positions of PDE5 backbone atoms from those in the initial structure. BL2 = HO^- (A) or H_2O (B).

etry. The Zn^{2+}-O(BL2) distance of 2.82 Å optimized with the electronic embedding charges is significantly longer than the normal equilibrium Zn^{2+}-O distance of 1.9 ~ 2.3 Å,[27] but it is significantly shorter than our previously optimized Zn^{2+}-O(BL2) distance of 3.58 Å.[27] Depicted in Figure 3 is a plot of the total energy (in Hartree) calculated at the B3LYP/6-31G* level for a partially optimized $Zn^{2+}(H_2O)_6$ complex structure versus the Zn^{2+}-O(H_2O) distance between the subsystem $Zn^{2+}(H_2O)_5$ and the sixth water molecule. The complex structure was optimized at the B3LYP/6-31G* level for each given value of the Zn^{2+}-O(H_2O) distance. Figure 3 shows a local minimum at the Zn^{2+}-O(H_2O) distance of ~2.09 Å and a saddle point at the Zn^{2+}-O(H_2O) distance of ~2.55 Å. The Zn^{2+}-O(BL2) distance of 2.82 Å optimized for the PDE5(BL2 = H_2O) structure is longer than that associated with the saddle point. So, the 2.82 Å is an intervenient distance between the coordination and non-coordination states, but is much closer to the non-coordination state. These different values of the Zn^{2+}-O(BL2) distance imply that optimized Zn^{2+}-O(BL2) distance of 2.82 Å might not be in a truly relaxed protein environment. A detailed check on the PDE5(BL2 = H_2O) geometry optimized with the electronic embedding charges revealed that some water molecules were very close to BL2 as shown in Figure 4. These solvent water molecules clearly blocked the way for BL2 leaving Zn^{2+} during the geometry optimization process, which helps to understand why the optimized Zn^{2+}-O(BL2) distance is only 2.82 Å.

To further account for the dynamics of the protein, we have carried out QM/MM geometry optimizations starting from different snapshots of an MD-simulated PDE5(BL2 = H_2O) structure. With the Mg^{2+}-O(BL2) and Zn^{2+}-O(BL2) distances constrained, the MD simulation was performed for 5 ns and a stable MD trajectory (from 3 ns to 5 ns) was obtained (see Fig. 5). The superimposition between the x-ray structure (1RKP) and the final snap-shot of the MD simulation is shown in Figure 6. After the MD simulation, the backbone atoms did not change too much, and RMSD for the backbone between the X-ray structure (1RKP) and the final snap-shot of the MD simulation is ~1.76 Å. The constrained MD simulation led to a relaxed protein environment which best fits the Mg^{2+}-O(BL2) and Zn^{2+}-O(BL2) distances determined by the X-ray diffraction. Eleven snapshots (i.e. snapshots No. 1 to No. 11) of the MD-simulated PDE5(BL2 = H_2O) structure were taken between 3 ns to 5 ns (one snapshot per 200 ps). Each snapshot was used as an initial structure of PDE5(BL2 = H_2O) to perform a QM/MM geometry optimization. The solvated PDE5(BL2 = H_2O) structure used in the QM/MM geometry optimization included all of the water molecules inside the protein and all of the water molecules within 2.5 Å from the surface outside the protein. Starting from these 11 snapshot structures, the QM/MM geometry optimizations were first carried out for all of the snapshots without the electronic embedding charges. To further examine the effects of the electronic embedding charges, we also performed the QM/MM geometry optimizations on three representative snapshots (No. 2, No. 6, and No. 11) with the electronic embedding charges. The QM/MM-optimized structures corresponding to these three representative snapshots are depicted in Figure 7. The optimized key distances are summarized in Table 1.

According to the optimized Mg^{2+}-O(BL2) and Zn^{2+}-O(BL2) distances in Table 1, the QM/MM geometry optimizations, with and without the electronic embedding charges, starting from all of the snapshots of the solvated PDE5(BL2 = H_2O) structure determined by the constrained MD simulation consistently demonstrate that BL2 only can coordinate Mg^{2+} with an Mg^{2+}-O(BL2) distance of 1.93 ~ 2.10 Å and a Zn^{2+}-O(BL2) distance

Figure 6. Superimposition between X-ray structure (1RKP, in yellow) and the final snap-shot of the MD simulation (other colors): (A) the backbone structures; (B) the active-site structures.

Figure 7. Geometries of PDE5(BL2 = H_2O) optimized by performing the QM/MM calculations with the electronic embedding charges at the B3LYP/6-31G*:Amber level. The initial structures used in the QM/MM geometry optimizations are the No. 2 (A), No. 6 (B), and No. 11 (C) snapshots of the trajectory for the constrained MD simulation on the PDE5(BL2 = H_2O) structure. The high-layer atoms are represented by the balls in colors other than yellow. The yellow balls represent the low-layer atoms of the residues coordinating the metal ions. The sticks refer to the solvent water molecules in the active site.

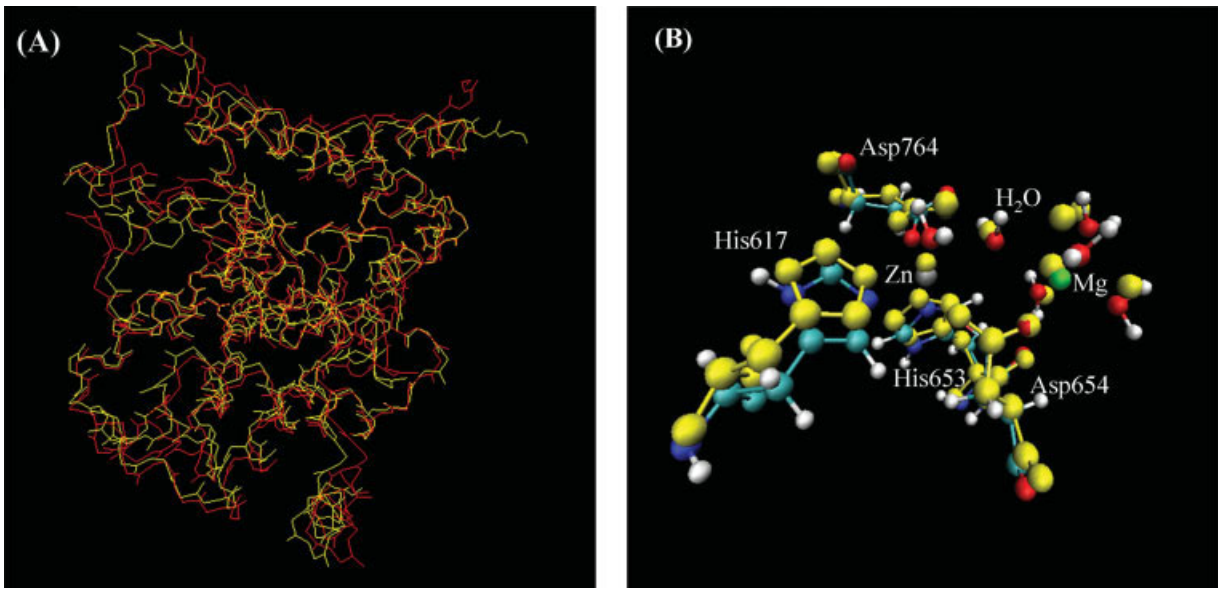

Figure 6

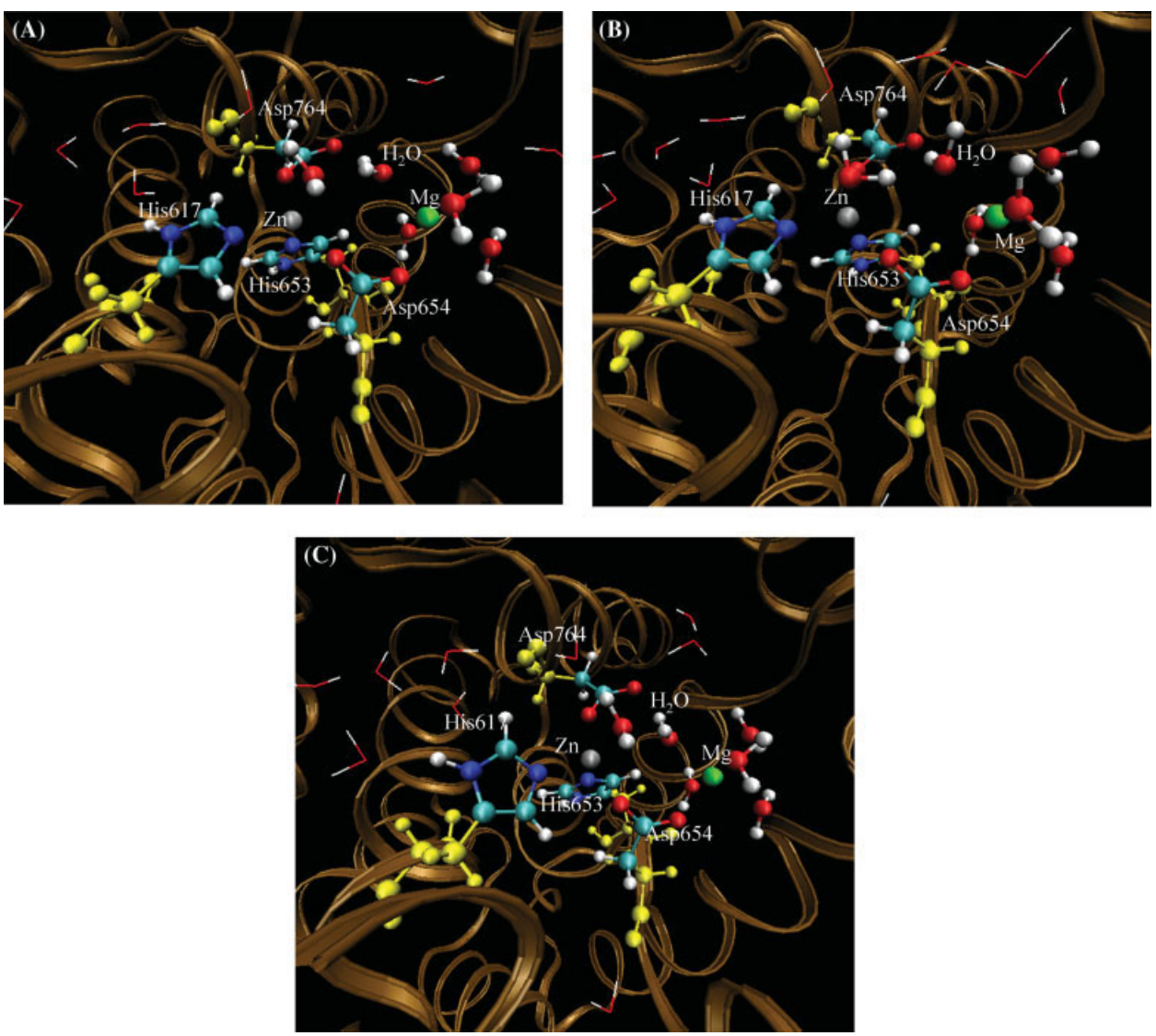

Figure 7

Table 1. The Internuclear Distances (Å) Between the BL2 Oxygen and Mg^{2+} and Between the BL2 Oxygen and Zn^{2+} and the Mg^{2+}-O(H_2O)-Zn^{2+} Angle in the QM/MM-Optimized Geometries of PDE5(BL2 = H_2O) and the Available X-ray Structure.

	Bond length[b]		Bond angle[b]
Method[a]	Mg^{2+}-O(H_2O)	Zn^{2+}-O(H_2O)	Mg^{2+}-O(H_2O)-Zn^{2+}
QM/MM-Ia[c]	2.00 (2.15)	3.58 (2.36)	103.70 (121.90)
QM/MM-Ib[d]	(2.07)	(3.28)	(112.93)
QM/MM-II[e]	2.00 (2.13)	4.05 (2.82)	99.04 (121.51)
QM/MM-MD[f]			
No. 1	2.03	3.89	100.25
No. 2	1.96 (2.04)	3.86 (3.35)	104.19 (107.15)
No. 3	1.98	3.95	100.73
No. 4	1.93	3.46	104.64
No. 5	1.99	3.93	104.75
No. 6	1.98 (2.10)	3.57 (3.44)	108.69 (108.59)
No. 7	1.98	3.58	113.62
No. 8	2.03	4.11	99.00
No. 9	1.99	4.03	103.60
No. 10	2.02	3.86	102.33
No. 11	1.99 (2.07)	3.58 (3.57)	108.43 (108.68)
Expt.[g]	2.37	2.54	110.14

[a]The geometries were fully optimized by performing the QM/MM calculations at the B3LYP/6-31G*:Amber level.

[b]The values in parentheses are the geometric parameters (Å and degree) obtained from the QM/MM geometry optimizations with the electronic embedding. The other data, i.e. those not in parentheses, are the geometric parameters obtained from the QM/MM geometry optimizations without the electronic embedding.

[c]QM/MM-Ia represents the QM/MM geometry optimization in the gas phase starting from the X-ray crystal structure and neglecting solvent water molecules that do not directly coordinate the metal ions.

[d]QM/MM-Ib represents the full QM/MM geometry optimization starting from the final partially optimized geometry at the final (12th) point in Figure 2.

[e]QM/MM-II refers to the full QM/MM geometry optimization starting from the X-ray crystal structure and including all of the resolved solvent water molecules in the calculation.

[f]QM/MM-MD means the full QM/MM geometry optimizations on the 11 snapshot structures (No. 1 to No. 11) obtained from the constrained MD simulation on the solvated PDE5(BL2 = H_2O) structure.

[g]From the X-ray crystal structure (PDB code 1RKP).

of 3.35 $\sim$ 4.11 Å. Hence, it does not matter whether the electronic embedding charges are included or not in the QM/MM geometry optimizations, so long as the solvent water molecules were accounted for and the constrained MD simulation was performed to relax the protein environment before the QM/MM geometry optimizations. The electronic embedding charges are important only when the QM/MM geometry optimizations are performed in the gas phase neglecting the solvent water molecules or ignoring the dynamics of the protein environment.

The Structure of PDE5(BL2 = HO^-)

The similar types of QM/MM geometry optimizations described for studying the PDE5(BL2 = H_2O) structure were also performed to examine the PDE5(BL2 = HO^-) structure. In all of the QM/MM-optimized geometries (not shown) of PDE5(BL2 = HO^-), BL2 (i.e. HO^-) always bridges the two positively charged metal ions (Zn^{2+} and Mg^{2+}), no matter whether the initial structure used for the QM/MM geometry optimization is the x-crystal structure or MD-simulated structure and no matter whether the solvent water molecules and electronic embedding charges are included in the QM/MM calculation or not. The results obtained from the current new QM/MM calculations confirm the previous conclusion[27] concerning the coordination of BL2 in the PDE5(BL2 = HO^-) active site.

In comparison between the optimized PDE5(BL2 = HO^-) structure and the optimized PDE5(BL2 = H_2O) structure, we can clearly see that only the optimized PDE5(BL2 = HO^-) structure is qualitatively consistent with the reported X-ray crystal structure. Hence, the X-ray crystal structure should be PDE5(BL2 = HO^-), rather than PDE5(BL2 = H_2O) and, therefore, the second bridge ligand (BL2) in the X-ray crystal structure should be HO^-, rather than H_2O. Because the crystal environment in the X-ray crystal structure only fits HO^- as BL2, when HO^- was replaced by a water molecule (H_2O) in the QM/MM geometry optimization without accounting for the dynamics of the protein environment, the water molecule tended to leave Zn^{2+} but could not go too far away from the initial position of HO^- which more tightly contacted with other water molecules nearby. The other water molecules nearby blocked the BL2 leaving during the QM/MM geometry optimization. The results obtained from these QM/MM geometry optimizations following the constrained MD simulation clearly demonstrate a dynamically stable PDE5(BL2 = H_2O) structure in solution in which BL2 only coordinates Mg^{2+}.

Conclusion

The extensive QM/MM geometry optimizations starting from the X-ray crystal structure and from the snapshot structures of the constrained MD simulations have clearly demonstrated two dynamically stable active site structures of PDE5, i.e. PDE5(BL2 = HO^-) and PDE5(BL2 = H_2O), in solution. It has been shown that the second bridging ligand (BL2, i.e. HO^-) in the PDE5(BL2 = HO^-) structure can really bridge the two positively charged metal ions (Zn^{2+} and Mg^{2+}) in the active site, whereas BL2 (i.e. H_2O) in the PDE5(BL2 = H_2O) structure can only coordinate Mg^{2+} and separates from Zn^{2+}. Only the optimized PDE5(BL2 = HO^-) structure is qualitatively consistent with the X-ray crystal structure in terms of the coordination of BL2, confirming that the second bridging ligand in the X-ray crystal structure of PDE5 should be HO^-, rather than H_2O.

It has been demonstrated that the results of the QM/MM geometry optimizations are significantly affected by the solvent water molecules, the dynamics of the protein environment, and the electronic embedding charges of the MM region in the QM part of the QMM/MM calculation. The PDE5(BL2 = H_2O) geometries optimized by using the QM/MM method in different ways show strong couplings between these important factors. It is interesting to note that the PDE5(BL2 = HO^-) and PDE5(BL2 = H_2O) geometries determined by the QM/MM calculations neglecting these three factors are all consistent with

the corresponding geometries determined by the QM/MM calculations that account for all of these three factors. These results suggest the overall effects of these three important factors on the optimized geometries can roughly cancel out. However, the QM/MM calculations that only account for some of these factors could lead to remarkably different geometries.

The results obtained from the present computational study are not only valuable for better understanding the PDE5 active site structures in the crystal structure and in solution, but also useful in guiding future QM/MM calculations on other enzyme systems.

References

1. Francis, S. H.; Lincoln, T. M.; Corbin, J. D. J Biol Chem 1980, 255, 620.
2. Thomas, M. K.; Francis, S. H.; Corbin, J. D. J Biol Chem 1990, 265, 14964.
3. Francis, S. H.; Turko, I. V.; Corbin, J. D. Prog Nucleic Acid Res Mol Biol 2001, 65, 1.
4. Liu, L.; Underwood, T.; Li, H.; Pamukcu, R.; Thompson, W. J. Cell Signal 2002, 14, 45.
5. Zoraghi, R.; Corbin, J. D.; Francis, S. H. Mol Pharmacol 2004, 65, 267.
6. Manganiello, V. Mol Pharmacol 2003, 63, 1209.
7. Murthy, K. S.; Zhou, H.; Makhlouf, G. M. Am. J. Physiol Cell Physiol 2002, 282, C508.
8. Conti, M.; Jin, S. L. C.; Monaco, L.; Repaske, D. R.; Swinnen, J. V. Endocr Rev 1991, 12, 218.
9. Teixeira, M. M.; Gristwood, R. W.; Cooper, N.; Hellewell, P. G. Trends Pharmacol Sci 1997, 18, 164.
10. Torphy, T. J.; Page, C. Trends Pharmacol Sci 2000, 21, 157.
11. Rotella, D. P. Nat Rev Drug. Discov 2002, 1, 674.
12. Reffelmann, T.; Kloner, R. A. Circulation 2003, 108, 239.
13. Zhang, K. Y.; Ibrahim, P. N.; Gillette, S.; Bollag, G. Expert Opin Ther Targets 2005, 9, 1283.
14. Houslay, M. D.; Sullivan, M.; Bolger, G. B. Adv Pharmacol 1998, 44, 225.
15. Corbin, J. D.; Francis, S. H. J Biol Chem 1999, 274, 13729.
16. Blount, M. A.; Beasley, A.; Zoraghi, R.; Sekhar, K. R.; Bessay, E. P.; Francis, S. H.; Corbin, J. D. Mol Pharmacol 2004, 66, 144.
17. Corbin, J. D.; Francis, S. H. Int J Clin Pract 2002, 56, 453.
18. Sebkhi, A.; Strange, J. W.; Phillips, S. C.; Wharton, J.; Wilkins, M. R. Circulation 2003, 107, 3230.
19. Sung, B. J.; Hwang, K. Y.; Jeon, Y. H.; Lee, J. I.; Heo, Y. S.; Kim, J. H.; Moon, J.; Yoon, J. M.; Hyun, Y. L.; Kim, E.; Eum, S. J.; Park, S. Y.; Lee, J. O.; Lee, T. G.; Ro, S.; Cho, J. M. Nature 2003, 425, 98.
20. Huai, Q.; Liu, Y.; Francis, S. H.; Corbin, J. D.; Ke, H. J Biol Chem 2004, 279, 13095.
21. Card, G. L.; England, B. P.; Suzuki, Y.; Fong, D.; Powell, B.; Lee, B.; Lu, C.; Tabrizizad, M.; Gillette, S.; Ibrahim, P. N.; Artis, D. R.; Bollag, G.; Milburn, M. V.; Kim, N. S.-H.; Schlessinger, J.; Zhang, K. Y. J. Structure 2004, 12, 2233.
22. Zhang, K. Y. J.; Card, G. L.; Suzuki, Y.; Artis, D. R.; Fong, D.; Gillette, S.; Hsieh, D.; Neiman, J.; West, B. L.; Zhang, C.; Milburn, M. V.; Kim, S.-H.; Schlessinger, J.; Bollag, G. Mol Cell 2004, 15, 279.
23. Senn, H. M.; Thiel, W. Top Curr Chem 2007, 268, 173.
24. Maseras, F.; Morokuma, K. J Comput Chem 1995, 16, 1170.
25. Ryde, U.; Olsen, L.; Nilsson, K. J Comput Chem 2002, 23, 1058.
26. Yu, N.; Hayik, S. A.; Wang, B.; Liao, N.; Reynolds, C.; Merz, K. M., Jr. J Chem Theory Comput 2006, 2, 1057.
27. Xiong, Y.; Lu, H.-T.; Li, Y.; Yang, G. -F.; Zhan, C.-G. Biophys J 2006, 91, 1858.
28. Frisch, M. J.; Trucks, G. W.; Schlegel, H. B.; Scuseria, G. E.; Robb, M. A.; Cheeseman, J. R.; Montgomery, J. A., Jr; Vreven, T.; Kudin, K. N.; Burant, J. C.; Millam, J. M.; Iyengar, S. S.; Tomasi, J.; Barone, V.; Mennucci, B.; Cossi, M.; Scalmani, G.; Rega, N.; Petersson, G. A.; Nakatsuji, H.; Hada, M.; Ehara, M.; Toyota, K.; Fukuda, R.; Hasegawa, J.; Ishida, M.; Nakajima, T.; Honda, Y.; Kitao, O.; Nakai, H.; Klene, M.; Li, X.; Knox, J. E.; Hratchian, H. P.; Cross, J. B.; Adamo, C.; Jaramillo, J.; Gomperts, R.; Stratmann, R. E.; Yazyev, O.; Austin, A. J.; Cammi, R.; Pomelli, C.; Ochterski, J. W.; Ayala, P. Y.; Morokuma, K.; Voth, G. A.; Salvador, P.; Dannenberg, J. J.; Zakrzewski, V. G.; Dapprich, S.; Daniels, A. D.; Strain, M. C.; Farkas, O.; Malick, D. K.; Rabuck, A. D.; Raghavachari, K.; Foresman, J. B.; Ortiz, J. V.; Cui, Q.; Baboul, A. G.; Clifford, S.; Cioslowski, J.; Stefanov, B. B.; Liu, G.; Liashenko, A.; Piskorz, P.; Komaromi, I.; Martin, R. L.; Fox, D. J.; Keith, T.; Al-Laham, M. A.; Peng, C. Y.; Nanayakkara, A.; Challacombe, M.; Gill, P. M. W.; Johnson, B.; Chen, W.; Wong, M. W.; Gonzalez, C.; Pople, J. A. Gaussian 03, Revision A. 1; Gaussian, Inc.: Pittsburgh, PA, 2003.
29. Bernstein, F. C.; Koetzle, T. F.; Williams, G. J.; Meyer, E. E., Jr; Brice, M. D.; Rodgers, J. R.; Kennard, O.; Shimanouchi, T.; Tasumi, M. J Mol Biol 1977, 112, 535.
30. Case, D. A.; Pearlman, D. A.; Caldwell, J. W.; Cheatham, T. E., III; Wang, J.; Ross, W. S.; Simmerling, C. L.; Darden, T. A.; Merz, K. M.; Stanton, R. V.; Cheng, A. L.; Vincent, J. J.; Crowley, M.; Tsui, V.; Gohlke, H.; Radmer, R. J.; Duan, Y.; Pitera, J.; Massova, I.; Seibel, G. L.; Singh, U. C.; Weiner, P. K.; Kollman, P. A. AMBER 7; University of California: San Francisco, 2002.
31. (a) Zhan, C.-G.; Norberto de Souza, O.; Rittenhouse, R.; Ornstein, R. L. J Am Chem Soc 1999, 121, 7279; (b) Koca, J.; Zhan, C.-G.; Rittenhouse, R.; Ornstein, R. L. J Am Chem Soc 2001, 123, 817; (c) Koca, J.; Zhan, C.-G.; Rittenhouse, R. C.; Ornstein, R. L. J Comput Chem 2003, 24, 368.
32. Berendsen, H. C.; Postma, J. P. M.; van Gunsteren, W. F.; DiNola, A.; Haak, J. R. J Comp Phys 1984, 81, 3684.
33. Ryckaert, J. P.; Ciccotti, G.; Berendsen, H. C. J Comp Phys 1977, 23, 327.
34. Darden, T.; York, D.; Pedersen, L. J Chem Phys 1993, 98, 10089.
35. (a) Dapprich, S.; Komaromi, I.; Byun, K. S.; Morokuma, K.; Frisch, M. J. J Mol Struct (Theochem) 1999, 461, 1; (b) Vreven, T.; Morokuma, K. J Chem Phys 2000, 113, 2969; (c) Vreven, T.; Morokuma, K.; Farkas, O.; Schlegel, H. B.; Frisch, M. J. J Comput Chem 2003, 24, 760.